

Effect of proton-amplified waves on the evolution of solar energetic particle composition in gradual events

Chee K. Ng,¹ Donald V. Reames,

Laboratory for High Energy Astrophysics, NASA Goddard Space Flight Center, Greenbelt, Maryland

Allan J. Tylka

Naval Research Laboratory, Washington, DC

Abstract

We present a model of the coupled evolution of energetic ions and Alfvén waves, incorporating magnetic focusing, pitch-angle diffusion, wave amplification, and a traveling ion source. Ion transport through proton-amplified waves with non-Kolmogorov spectra produces the contrasting three-stage evolution of Fe/O and He/H ratios at several MeV/amu observed by Wind/EPACT in the 20 April 1998 gradual solar energetic particle event [*Tylka et al.*, 1999].

¹Also at Department of Astronomy, University of Maryland, College Park

Introduction

Cliver [1996], *Gosling* [1993], *Kahler* [1992], *Lee* [1997], and *Reames* [1997] have reviewed various observations and arguments in support of the scenario that solar energetic particles (SEPs) in gradual events are accelerated from suprathermal solar-wind ions by a traveling interplanetary shock driven by a fast coronal mass ejection (CME). For diffusive shock acceleration to apply, the SEPs must be scattered rapidly by waves near the shock. Near the sun the SEPs are strongly focused into beams which rapidly amplify Alfvén waves to great intensities, so that the waves in turn quickly scatter the SEPs [*Ng and Reames*, 1994]. The enhanced scattering near a shock dramatically increases its acceleration efficiency, so that a quasi-equilibrium is soon established between ion densities and streaming on the one hand and wave intensities and growth rates on the other [*Lee*, 1983, 1997].

Alfvén wave generation at a distance is unobservable. However, SEPs arriving at a spacecraft carry information on their past interaction with the waves. Careful study of the SEPs may thus provide indirect evidence for wave excitation and diffusive shock acceleration near the sun. *The key observation here is the SEP abundance histories.* Two ion species with unequal charge-to-mass ratios A/Q and *the same velocity* interact resonantly with Alfvén waves of different wavelengths. The resulting difference in their acceleration and transport is sensitively reflected in their abundance ratio history.

Observation of the remarkable SEP abundance evolution by Wind/EPACT in gradual events is presented in the companion *Letter* by *Tylka et al.* [1999]. We concentrate here on the 2.5-3.2, 3.2-5.0, and 5-10 MeV/amu Fe/O ratios, normalized to coronal values, and the normalized 2.0-2.5 MeV/amu He/H ratio in the 1998 April 20 *west limb* event. We identify the following salient features in the Fe/O histories: (1) a precipitous initial decay from large values to energy dependent values $\gtrsim 1$, (2) a less rapid rebound to an energy dependent peak (> 1), and (3) a monotonic decrease to energy dependent values $\lesssim 1$. In sharp contrast, He/H almost mirrors 2.5-3.2 MeV/amu Fe/O about the unit ratio – rising when Fe/O descends, and descending when Fe/O rises away from unity. The difference between He/H and Fe/O histories has been noted before [e.g. *Mason et al.*, 1983].

This *Letter* is a report on our preliminary study of these *concurrent* abundance histories using a model of the coupled evolution of SEPs and Alfvén waves. Comparison of model prediction and observation in the 20 April 1998 west limb event supports the key role played by proton excited waves in near-Sun diffusive shock acceleration and inter-

planetary transport of SEPs in gradual events.

Model

No theoretical model treats SEP acceleration and transport near its full complexity. The many difficulties involved are described in *Lee* [1997] and *Lee and Ryan* [1986]. A spacecraft samples in time progressively more eastern corotating flux tubes (CFTs), each with a distinct history of shock parameters [*Cane et al.* 1988; *Reames et al.*, 1996]. To model the SEP intensity histories at a spacecraft, we should likewise step through a long sequence of individual solutions on different CFTs. Fortunately, in a *west limb* event the sequence progresses eastward toward weaker and slower shocks, and we may use the solution on just *one* intermediate CFT to approximate the real intensity evolution, albeit on a distorted time scale. We adopt this simplified approach in this *Letter*.

The model here extends the work of *Ng and Reames* [1994] on the coupled evolution of SEPs and Alfvén waves to include a traveling source of energetic ions. Several simplifying assumptions have been made to render the model tractable. Ion acceleration is accounted for crudely and decoupled from transport by injecting time varying power-law spectra of accelerated ions [*Lee*, 1983] at the “shock”, which travels radially at constant velocity V_{sh} , its heliocentric distance at time t thus given by $r_{sh} = r_{0,sh} + tV_{sh}$. Ion transport includes pitch-angle scattering and focusing by a radial magnetic field but ignores solar-wind convection and energy change. Wave evolution is due to amplification by streaming protons only, and all other processes, e.g. wave transport and cascading, are ignored.

The phase space densities $f_s(\mu, P, r, t)$ of ion species s and the differential wave intensities $I_\sigma(k, r, t)$ of wave mode σ are governed by [*Ng and Reames*, 1994]

$$\frac{\partial f_s}{\partial t} + \mu v \frac{\partial f_s}{\partial r} + \frac{1 - \mu^2}{r} v \frac{\partial f_s}{\partial \mu} - \frac{\partial}{\partial \mu} \left(D_{\mu\mu}^s \frac{\partial f_s}{\partial \mu} \right) = G_s \quad (1)$$

$$\frac{\partial I_\sigma(k, r, t)}{\partial t} = \gamma_\sigma(k, r, t) I_\sigma(k, r, t) \quad (2)$$

$$D_{\mu\mu}^s = \frac{v^2}{4P^2} \sum_\sigma \int dk I_\sigma(k, r, t) R_{\mu\mu}^\sigma(\mu, v, P, k, V_\sigma) \quad (3)$$

$$\gamma_\sigma = 2\pi^2 g_\sigma e^3 c V_A \iint d\mu dP \frac{P^3}{E^2} \frac{R_{\mu\mu}^\sigma}{(1 - \mu V_\sigma/v)^2} \frac{\partial f_H}{\partial \mu} \quad (4)$$

In the above, r is heliocentric distance, v ion velocity, P rigidity, μ pitch-angle cosine, $D_{\mu\mu}^s(P, \mu, r, t)$ μ -space diffusion coefficient of species s , k wavenumber, G_s ion “source” term, γ_σ growth rate of I_σ , c light speed, e elementary charge, E proton total energy, V_A Alfvén speed, V_{SW}

solar-wind speed, $g_\sigma = \pm 1$ for outward (inward) waves, $V_\sigma = V_{\text{SW}} + g_\sigma V_A$, and $R_{\mu\mu}^\sigma(\mu, v, P, k, V_\sigma)$ wave-particle resonance function [Ng and Reames, 1995]. Compared to protons, the minor ions contribute negligibly to wave evolution [Lee, 1983]. Hence only f_H appears in eq. (4). Eq. (1) for f_H and eq. (2) for I_σ are coupled by virtue of eqs. (3) and (4).

The moving ion source G_s per ($\text{cm}^3 \text{ MV}^3 \text{ hr}$) is assumed isotropic and sharply peaked at $r = r_{\text{sh}}$, such that

$$\frac{1}{\Delta r} \int_{r_{\text{sh}} - \frac{1}{2}\Delta r}^{r_{\text{sh}} + \frac{1}{2}\Delta r} G_s dr = \alpha \delta \frac{n_s(r_0) r_0^2}{P_{0,s}^3 r_{\text{sh}}^2} \left(\frac{P}{P_{0,s}} \right)^{-\delta} \quad (5)$$

and G_s is negligible outside the above interval, with Δr the finite-difference grid size. In eq. (5), $n_s(r_0) r_0^2 / r^2$ is the solar-wind s -ion density at r , $r_0 \equiv 1 \text{ AU}$, $P_{0,s}$ is the “seed” ion rigidity, and the parameter α depends inversely on the acceleration time. We take $n_H(r_0) = 6.4 \text{ cm}^{-3}$, a typical observational value at $r = 1 \text{ AU}$, with $n_O(r_0) = 4.1 \times 10^{-3} \text{ cm}^{-3}$ and $n_{\text{Fe}}(r_0) = 5.5 \times 10^{-4} \text{ cm}^{-3}$, in proportion to the observed coronal abundances [Reames, 1995]. All ions are seeded at 5 keV/amu [Lee, 1983].

For the 20 April 1998 event, we adopt the following. $V_{\text{sh}} = 1250 \text{ km s}^{-1}$, between the observed CME speed of $\approx 1600 \text{ km s}^{-1}$ [C. St. Cyr, private communication] and the shock’s mean transit speed of $\approx 520 \text{ km s}^{-1}$. $V_{\text{SW}} = 417 \text{ km s}^{-1}$. $V_A = (41.7 \text{ km s}^{-1})(r_0/r)$. A softening spectrum: $\delta = \delta_0 + V_{\text{sh}} t \delta'$, with $\delta_0 = -4$, $\delta' = -2.5 \text{ AU}^{-1}$, implying that the shock compression ratio weakens from 4 at $r = 0.01125 \text{ AU}$, $t = 0 \text{ hr}$ to 1.86 at $r = 1.125 \text{ AU}$, $t = 33 \text{ hr}$. $A_{\text{Fe}}/Q_{\text{Fe}} = 4$, $A_{\text{O}}/Q_{\text{O}} = A_{\text{He}}/Q_{\text{He}} = 2$. For all species, $\alpha = 8 \times 10^{-5} \text{ hr}^{-1}$.

The *initial* forward Alfvén wave distributions are specified via eq. (27) of Ng and Reames [1994] with (*symbols therein*) $I_{+0} = 1 \times 10^{-3} \text{ MeV cm}^{-2}$, $\delta = -5/3$, and $\gamma = 0.015 \text{ hr}^{-1}$. Backward wave intensities are 10% of the forward wave intensities. The resulting mean free paths $\lambda \gtrsim 1 \text{ AU}$ for the ions of interest, where $\lambda = 3/8 \int_{-1}^1 d\mu (1 - \mu^2)^2 v / D_{\mu\mu}$ [Earl, 1974].

The coupled eqs. (1) and (2) are solved using a refinement of the finite-difference technique of Ng and Reames [1994], subject to the above initial wave distributions, zero initial ion densities, a reflecting inner boundary at $r = 0.1 \text{ AU}$, and a free-escape outer boundary at $r = 2.6 \text{ AU}$. The rigidity range is from 16 MV to 609 MV. We select $r = 1.125 \text{ AU}$ for “observation” to compensate for the assumed radial magnetic field line.

Results

Abundance Ratio Evolution

In quasi-linear theory, $I_\sigma(k) \propto k^{-5/3}$ implies $D_{\mu\mu}/v \propto P^{-1/3}$ and $\lambda \propto P^{1/3}$, roughly. Thus at the same velocity and twice the rigidity, Fe^{14+} (He^{2+}) suffers less scattering than O^{8+} (H^+). Relatively more Fe^{14+} (He^{2+}) than O^{8+} (H^+) ions would arrive at first, leading to a large Fe/O (He/H) ratio at onset, followed by a rapid decrease of the ratio as more O^{8+} (H^+) ions arrive later. This prediction is observed for Fe/O, but in contradiction to the observed He/H history in the 1998 April 20 event (see Introduction and Figure 2 of Tylka et al. [1999]).

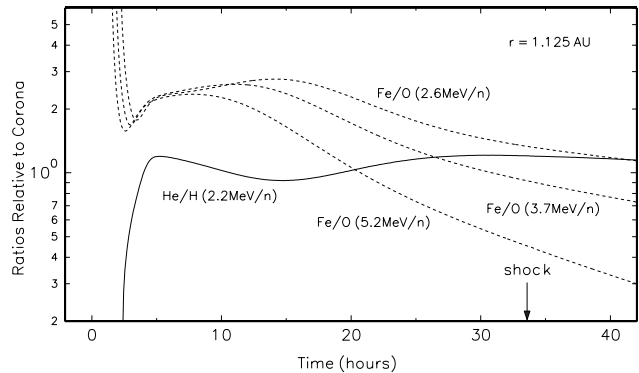


Figure 1: Fe/O and He/H ratios at $r = 1.125 \text{ AU}$, showing the three evolutionary phases (see text). The shock arrival time at $r = 1.125 \text{ AU}$ is indicated by an arrow.

Figure 1 shows the predicted histories of 2.6, 3.7, and 5.2 MeV/amu Fe/O and 2.2 MeV/amu He/H ratios at $r = 1.125 \text{ AU}$. Remarkably, the model produces qualitatively the observed three-phase time profiles, in particular, the contrast between He/H and Fe/O. This is due to (r, t) -dependent wave amplification by streaming protons. Protons that resonate with the same waves as He^{2+} or O^{8+} (Fe^{14+}) travel at twice (quadruple) the speed of the latter ions. At event start, the faster protons race ahead and amplify the resonant waves, enhancing the scattering condition for the heavier ions even *before* the latter’s first arrival. Because of the decreasing proton rigidity spectrum, this initial disturbance does not cause more scattering of Fe^{14+} than O^{8+} . However, the radial profiles of $D_{\mu\mu}^{\text{He}}/D_{\mu\mu}^{\text{H}}$ at $\mu = 0.9$ in Figure 2 show that the faster proton outriders generate a moving shell of disturbance, in which the first “wave” of He^{2+} are pitch-angle scattered faster than the first “wave” of H^+ at $\mu \gtrsim 0.8$, leading, at $r = 1.13 \text{ AU}$, to

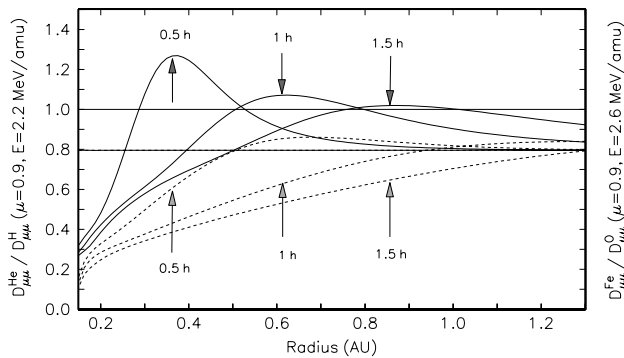


Figure 2: Radial profiles of 2.2 MeV/amu $D_{\mu\mu}^{He}/D_{\mu\mu}^H$ (solid curves) and 2.6 MeV/amu $D_{\mu\mu}^{Fe}/D_{\mu\mu}^O$ (dashed curves) at $\mu = 0.9$. An arrow indicates both time of profile and farthest point reached by the ions.

He/H that rises rapidly from small values at onset. What causes the slower rebound of Fe/O (the slower fall of He/H) in the second phase? Without wave growth, one expects the ratio to approach an asymptotic value from above, contrary to the observation. Proton-driven wave growth, however, causes the ion mean free paths λ_{Fe} and λ_O to fall in time and to increase with distance upstream from the shock, such that $\lambda_{Fe} > \lambda_O$ everywhere. Figure 3 shows the radial profiles of λ_O at 2.6 MeV/amu at selected times. Figure 4a shows the radial profiles of λ_{Fe}/λ_O and λ_{He}/λ_H at $t = 3$ hr, 12 hr, and 24 hr. The corresponding radial profiles of Fe/O at 2.6 MeV/amu and He/H at 2.2 MeV/amu are shown in Figure 4b. Since $\lambda_{Fe} > \lambda_O$ everywhere, relatively more Fe^{14+} than O^{8+} arrive from the shock, and Fe/O rebounds in the second phase. In a fairly extensive region starting

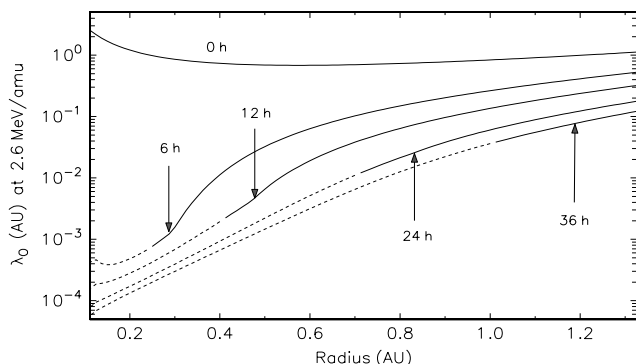


Figure 3: Radial profiles of λ_O at 2.6 MeV/amu. Arrow indicates time of profile and shock location. Profiles far behind the shock should not be taken seriously because of the neglect of convection and wave transport.

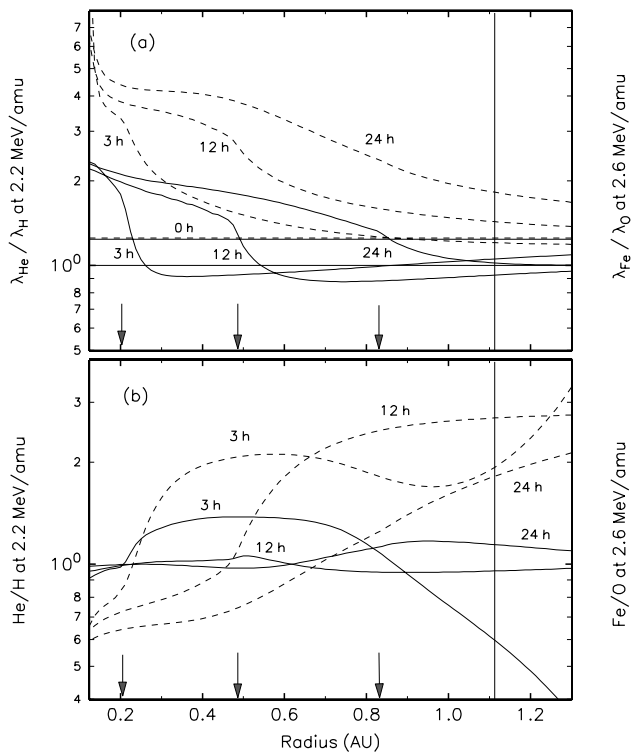


Figure 4: Radial profiles of (a) the mean-free-path ratios and (b) the abundance ratios, for He to H at 2.2 MeV/amu and Fe to O at 2.6 MeV/amu at selected times.

a short distance beyond the shock, $\lambda_{He} < \lambda_H$ (Figure 4a); He^{2+} experiences more scattering en route than H^+ , and so He/H falls in time.

The third phase sees Fe/O fall and He/O rise as the shock approaches. This is again consistent with proton driven wave growth. As shown in Figure 4, $\lambda_{Fe} > \lambda_O$ ($\lambda_{He} < \lambda_H$) goes generally with a positive (negative) radial gradient of Fe/O (He/H). As the shock approaches, the spacecraft eventually enters a region where Fe/O (He/H) is smaller (larger) than before.

Wave Evolution

We display in Figure 5 the evolution of the outward right-hand polarized Alfvén waves at $r = 0.35$ AU from an initial $k^{-5/3}$ spectrum. Wave growth occurs first at low k , then progresses to high k , reflecting the earlier arrival of faster protons. The growth rate is large early but decreases with time. Quasi-linear theory predicts $D_{\mu\mu}/v \propto P^{-2} I_R^+(k_{res})$ roughly, where $k_{res} \approx B/(\mu P)$, with B the magnetic field. If $I_R^+(k) \propto k^{-b}$, then $D_{\mu\mu}/v \propto P^{b-2}$, decreasing (increasing) with P if b is $<$ ($>$) 2. A k^{-2} spectrum is shown in Figure 5 for comparison. The initial $k^{-5/3}$

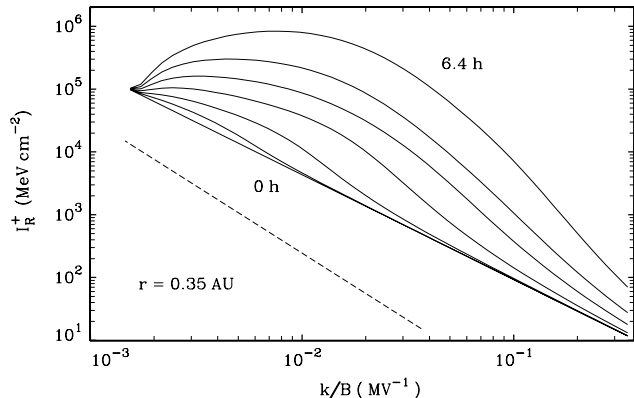


Figure 5: I_R^+ versus k/B at $r = 0.35$ AU and $t = 0, 0.2, 0.4, 0.8, 1.6, 3.2,$ and 6.4 h. A k^{-2} spectrum (dashed line) is shown for comparison.

wave spectra imply $D_{\mu\mu}/v \propto P^{-1/3}$ everywhere. However, wave evolution soon rewrites the rigidity dependence of $D_{\mu\mu}/v$, so that it decreases and increases with P at different values of P in an (r, t) -dependent manner. Similarly, λ and its rigidity dependence also evolve dynamically in response to wave growth. One may speculate that this effect contributes to event-to-event fluctuation in λ , with smaller λ going with larger proton events.

Particle Spectra

Figure 6 shows the differential intensities j_P^H , j_P^O , j_P^{Fe} versus rigidity P at $t = 30$ h. These spectra flatten at low rigidities, similar to the observation [Figure 3, *Tylka et al.*, 1999], because of the rigidity-dependent escape of the ions through proton-excited waves. At the same MeV/amu

$$\text{Fe/O} = [(A_{\text{Fe}}/Q_{\text{Fe}})/(A_{\text{O}}/Q_{\text{O}})] j_P^{\text{Fe}}(P_{\text{Fe}})/j_P^{\text{O}}(P_{\text{O}}).$$

Hence the spectral flattening implies that $^{16}\text{O}^{8+}$ is suppressed more than $^{56}\text{Fe}^{14+}$, as shown by the symbols in Figure 6 for 5.2 MeV/amu Fe and O.

Discussion

A sufficiently large initial proton “injection” rate is required in the model to produce the observed trend of He/H and Fe/O. Reducing G_H eventually results in He/H and Fe/O both decreasing from initially large values, contrary to the observation. Similar results to Figure 1 are obtained with Q_O from 6 to 8 and Q_{Fe} from 11 to 14.

Adopting a decreasing shock speed on each CFT and stepping through a sequence of CFTs toward slower and weaker shocks would allow the model to match the observed time scale of evolution. However, such refinements are not

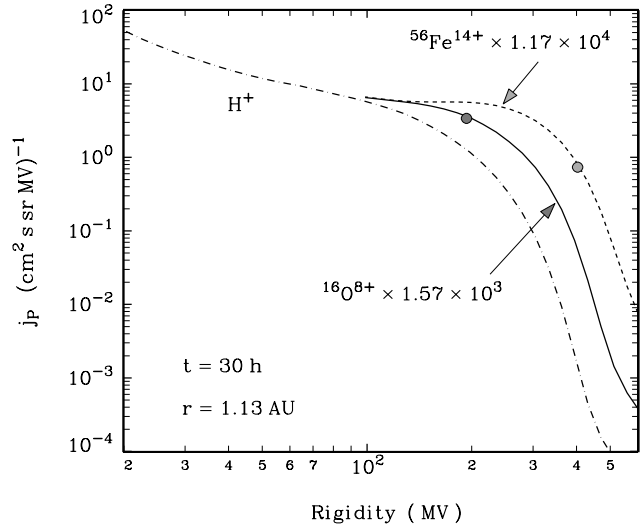


Figure 6: j_P^H , j_P^{Fe} , and j_P^{O} versus P at $r = 1.125$ AU, $t = 30$ h. The Fe and O spectra have been divided by their respective coronal abundances relative to H. Solid circles indicate values used to calculate 5.2 MeV/amu Fe/O.

warranted at present because we have neglected solar-wind convection, adiabatic deceleration, wave k -transport, and non-linear wave cascading.

The time scale for convection, adiabatic deceleration, and wave k -transport are, respectively, $1 \text{ AU}/V_{\text{sw}} \sim 100$ hr, $r/[(1-\mu^2)V_{\text{sw}}] \gtrsim 10$ hr, and $r/(2V_{\text{sw}}+3V_A) \gtrsim 2$ hr. These processes are unlikely to alter our conclusion. It is difficult to estimate the effect of non-linear cascading without actual modeling. We are generalizing our model to include these processes, and will report some preliminary results at the 26th International Cosmic Ray Conference. Despite simplifications, the model produces the contrasting three-phase Fe/O and He/H histories in the 20 April 1998 event, demonstrating the key role of proton excitation of Alfvén waves in SEP acceleration and transport.

The model may be used to study the evolution of charge state distributions via A/Q-dependent transport through SEP excited waves.

Acknowledgments. We thank M. A. Lee and T. T. von Rosenvinge for discussions, and the referees for helpful comments. AJT was supported by NASA DPR-S92662F.

References

Cane, H. V., Reames, D. V., and T. T. von Rosenvinge, The role of interplanetary shocks in the longitude distribution of solar energetic particles, *J. Geophys. Res.* 93, 9555-9567, 1988.

- Cliver, E. W., Solar flare gamma-ray emission and energetic particles in space, in *High Energy Solar Physics*, eds. R. Ramaty *et al.*, *AIP Conf. Proc.* 374 (AIP Press), 45-60, 1996.
- Earl, J. A., The diffusive idealization of charged-particle transport in random magnetic fields, *Astrophys. J.* 193, 231, 1974.
- Gosling, J. T., The solar flare myth, *J. Geophys. Res.* 98, 18937-18949, 1993.
- Kahler, S., Solar flares and coronal mass ejections, *Annu. Rev. Astron. Astrophys.* 30, 113-141, 1992.
- Lee, M. A., Coupled hydromagnetic wave excitation and ion acceleration at interplanetary shocks, *J. Geophys. Res.* 88, 6109-6119, 1983.
- Lee, M. A., Particle acceleration and transport at CME-driven shocks, in *Coronal Mass Ejections*, eds. N. Crooker, J. A. Jockelyn, and J. Feynman, *Geophys. Monograph* 99 (AGU Press) 227-234, 1997.
- Lee, M. A., and J. M. Ryan, Time-dependent coronal shock acceleration of energetic solar flare particles, *Astrophys. J.* 303, 829-842, 1986.
- Mason, G. M., Gloeckler, G., and D. Hovestadt, Temporal variations of nucleonic abundances in solar flare energetic particle events. I. well-connected events, *Astrophys. J.* 267, 844-862, 1983.
- Ng, C. K., and D. V. Reames, Focused interplanetary transport of ~ 1 MeV solar energetic protons through self-generated waves, *Astrophys. J.* 424, 1032-1048, 1994.
- Ng, C. K., and D. V. Reames, Pitch angle diffusion coefficient in an extended quasi-linear theory, *Astrophys. J.* 453, 890-905, 1995.
- Reames, D. V., Coronal abundances determined from energetic particles, *Adv. Space Res.* 15, 41-51, 1995.
- Reames, D. V., Energetic particles and the structure of coronal mass ejections, in *Coronal Mass Ejections*, *ibid*, 217-226, 1997.
- Reames, D. V., Barbier, L. M., and C. K. Ng, The spatial distribution of particles accelerated by coronal mass ejection-driven shocks, *Astrophys. J.* 466, 473-486, 1996.
- Tylka, A. J., Reames, D. V., and C. K. Ng, Observations of systematic temporal evolution in elemental composition during gradual solar energetic particle events, *Geophys. Res. Lett.* this issue, 1999.

C. K. Ng and D. V. Reames, Code 661, NASA Goddard Space Flight Center, Greenbelt, MD 20771 (e-mail: cheeng and reames@lheavx.gsfc.nasa.gov)

A. J. Tylka, Code 7654, E.O. Hulburt Center for Space Science, Naval Research Laboratory, Washington, DC 20375 (e-mail: tylka@cr2.nrl.mil)

Received March 17, 1999; accepted May 13, 1999.